

Application of a Signal Technique to the Source–Receptor Relationship in Three-Dimensional Tracer Simulations

ZHAN ZHAO AND SHU-HUA CHEN

Department of Land, Air, and Water Resources, University of California, Davis, Davis, California

(Manuscript received 3 November 2009, in final form 1 April 2010)

ABSTRACT

Identifying pollutant sources that contribute to downstream locations is important for policy making and air-quality control. In this study, a computationally economic signal technique was implemented into a three-dimensional nonhydrostatic atmospheric model to help to identify source–receptor relationships. An idealized supercell case and a semireal air-pollution case in Turkey were used to investigate the potential of the technique. For each pollutant, signals with various frequencies were emitted from different source locations and added into that particular type of emitted pollutants. The time series of pollutant concentration collected at receptors were then projected onto frequency space using the Fourier transform and short-time Fourier transform methods to identify the source locations. During the model integration, a particular tracer was also emitted from each pollutant source location (i.e., a conventional method to study the source–receptor relationship) to validate and evaluate the signal technique. Results show that frequencies could be slightly shifted after signals were transported for some distance and that evident secondary frequencies (i.e., beat frequencies) could be generated as a result of nonlinear effects. Although these could potentially confuse the identification of signals released from source points, signals were still distinguishable in this study. Results from a sensitivity test of the diffusion effect on different frequencies suggest that the effect of diffusion on amplitude damping is stronger for higher frequencies than for lower frequencies.

1. Introduction

The increase of population and industrial and commercial activities has exacerbated air-pollution problems. Of greatest concern to the public are the adverse health effects of most pollutants (Dockery and Pope 1994; Brunekreef and Holgate 2002). Airborne pollutants, especially fine particulate matter (PM) with aerodynamic diameter smaller than $2.5 \mu\text{m}$ ($\text{PM}_{2.5}$), have significant health impacts since they can be deeply inhaled with potentially toxic effects on the heart and lungs (Pope et al. 1995; Seaton et al. 1995); PM can also adversely affect visual range and ecosystems (EPA 1996).

Air pollutants and their precursors can be transported over great distances before being deposited at downstream receptors (Jaffe et al. 1999; Berntsen et al. 1999). Potential emission-control strategies often rely on determining proper source–receptor relationships using

air-quality models. For source-oriented Eulerian air-quality models (Peters et al. 1995; Kleeman et al. 1999), tracers, representing the pollutants, are emitted from the source points and propagate with the wind. Their paths are tracked by calculating the tracer concentrations in each grid cell of the model. An Eulerian model can be closely coupled with a meteorological model, whose outputs drive the tracers' transport, with both models having the same domain and grid spacing.

The tracer's transport and diffusion computations can be conducted within the meteorological model, known as an online approach (Grell et al. 2005; Chen et al. 2008a), or offline (Fox 1981; Held et al. 2005), whereby the meteorological output is saved at a suitable interval for later ingest into the transport model. The two approaches are identical when the meteorological model's output is stored at each time step (typically on the order of minutes) for use in the offline model. However, this is impractical, and wind output is typically saved on the order of hours. Temporal interpolation between available output times is one of the primary errors in air-pollution calculations (Stohl et al. 1995; Seaman 2000). Additional errors can arise from spatial interpolation

Corresponding author address: Dr. Shu-Hua Chen, Dept. of Land, Air, and Water Resources, University of California, Davis, 1 Shields Ave., Davis, CA 95616.
E-mail: shachen@ucdavis.edu

and inconsistent physics parameterization schemes between the two models (Stohl 1998). By implementing the tracer conservation equation into the meteorological model, the online approach can avoid the aforementioned errors. In addition, this method can take into account the effects of subgrid-scale convective mixing and subgrid-scale turbulent mixing, consistent with meteorological scalars (Chen et al. 2008a). However, each pollutant species from each source location is treated as one variable within the online model, and, therefore, using different tracers to represent different species and emission locations to find a unique source–receptor relationships can be computationally costly in both time and memory for a large airshed case (Held et al. 2005). For example, if there are N source points, with M species emitted from each source location, there would be $M \times N$ extra variables added to the model. Thus, this approach needs tremendous computational memory and time for a big-airshed case. The implementation of a signal technique (Hsu and Chang 1987) into this online approach can solve this problem to some degree. The main concept of this signal technique, as described in Hsu and Chang (1987), is that a unique oscillatory signal is superimposed onto emission data at each source point and propagates with the tracers; the frequency spectrum is obtained by analyzing the time series of pollutant concentration at the receptors. Because each source point was tagged with a unique frequency of the oscillatory signal, it is expected that the source–receptor relationship could potentially be identified from the spectrum at the receptor. By using different frequencies superimposed on tracers to represent different emission locations instead of using different tracers, the number of tracers needed in the model can be reduced (i.e., reduce computational time and memory). For the example mentioned before, instead of $M \times N$, only M new variables need to be added to the model. The objective of this study is to develop the Weather Research and Forecasting (WRF) tracer model, in which an online tracer calculation algorithm with signal-processing techniques was implemented, to study the signal technique in three-dimensional (3D) air-pollution applications. Two cases studies, an idealized 3D supercell case and a semi-real air-pollution case, are used to examine and demonstrate the signal technique. In the semi-real case study, instead of real emission sources (big cities), tracers are emitted from preselected sources within the limited WRF domain, because of the great computational demand for a real case that encompasses big cities (more details in section 4).

The paper is organized as follows: The method, numerical modeling, and time series analysis tools are described in section 2. An idealized-case experiment

and analysis are presented in section 3, and a semi-real-case experiment and results are presented in section 4. Concluding remarks are given in section 5.

2. Description of method and numerical modeling

a. Review of the signal technique

In theory, online tracer simulations can estimate the source–receptor relationships more accurately than can offline ones, at the expense of computational memory. Hsu and Chang (1987) proposed a signal technique to alleviate the computational burden of the online tracer method. In their experiments, a unique oscillatory signal S was superimposed onto emission data (i.e., tracers) with the form (1) at each source point:

$$S = \sum_i [E_i + A_i \sin(\omega_i t)] \delta(x - x_i), \quad (1)$$

where E_i is the constant tracer at location x_i , A_i is the amplitude of the artificial signal, $\omega_i = 2\pi(N_i/T)$ is the frequency, and $\delta(x - x_i)$ is the Dirac delta function.

Considering advection and diffusion processes, which are the two main atmospheric physical processes that affect the pollutant concentration, the governing equation for a nonreactive tracer in the x direction can be written as

$$\frac{\partial C}{\partial t} + U \frac{\partial C}{\partial x} = \nu \frac{\partial^2 C}{\partial x^2} + \sum_i [E_i + A_i \sin(\omega_i t)] \delta(x - x_i), \quad (2)$$

where U is the wind speed (set to be constant in their experiment) and ν is the Fickian diffusion coefficient. The analytic solution of Hsu and Chang (1987) at the receptor x in such a system indicates that 1) the leading frequency is the emitting frequency ω_i , 2) both processes can contribute to a phase shift $[\omega_i(x - x_i)/U]$ due to advection and $\pi/4$ due to diffusion], and 3) the amplitude modulation factors from advection and diffusion are $2 \cos[\omega_i(x - x_i)/U]$ and $(\gamma\omega_i)^{-1/2}$ respectively. Please refer to Hsu and Chang (1987) for details about deriving the analytic solutions.

In the numerical experiment, the signal propagation went through the same advective and diffusive processes as tracers in the numerical model. At the receptors, the frequency spectrum was obtained by analyzing the time series of pollutant concentration using a Fourier transform (FT). The spikes in the spectrum implied that signals with those frequencies were received at the analyzing receptors. Because each source point was tagged with a unique frequency of oscillatory signal,

the source–receptor relationships could potentially be identified from the spectrum at the receptor if there were no numerical error and if signals were not entirely diffused away. Several experiments were done for both nonreactive and reactive tracers with linear and weak nonlinear transformations, and their results were very promising. The signals could be detected at the receptors for all of the cases, although obvious “beat” signals were present for the weak nonlinear cases with mean background concentration. The sensitivities of the results to the diffusion effect and background concentration were also investigated. Consistent with the analytic solution, the diffusion effect on the amplitude response in the experiment is dependent on both the distance between the source and the receptor and the oscillation frequency (i.e., the higher the frequency is, the more the signal is diffused out). The generation of beat signals due to the mean background concentration could be reduced by choosing a proper signal strength.

The selection of the signal frequency is important. Hsu and Chang (1987) pointed out that the damping of the signal amplitude by the diffusion effect is proportional to the frequency. Therefore, frequencies that are too high should be avoided for this approach. It is possible that a slight shift of frequency and a spread of the frequency width could occur. The frequency shift is somewhat analogous to the Doppler shift, resulting from the nonlinear winds between the signal-emitting points and the receptors during the transport time. Shifting to higher frequencies means that the overall wind speed during the signal transport is higher than that at the source point when the signals are emitted, and vice versa. The dent between two contiguous spectrum peaks, which correspond to two signals, in the frequency space may become obscure because of frequency spread, and, therefore, the interval between two frequencies needs to be wide enough to reduce the ambiguity when doing spectrum analysis. Moreover, to apply this signal approach to the real atmosphere, one should avoid using the frequencies that already exist in the atmosphere, such as gravity waves, diurnal waves, and so on, so as to identify the frequencies from the signals.

The model used in Hsu and Chang (1987) is an idealized horizontal two-dimensional (2D) Eulerian numerical model, with a constant flow of 20 m s^{-1} . To evaluate this technique further, more studies using a realistic and sophisticated atmospheric model are required.

b. The approach

Tracers’ transport is mainly determined by the wind and the instability of the atmosphere. The performance of the signal technique in the real atmosphere, which has

a complex wind field, can be very different from that of the simple, constant-wind 2D model simulation in Hsu and Chang (1987). Thus, we propose to use a fully compressible 3D nonhydrostatic model with higher-order-accuracy numerical schemes to investigate the signal technique. The primary objective of this research is to investigate whether this signal technique is still capable of solving the source–receptor relationships for 3D nonlinear idealized cases and for pseudoreal cases within a complex model. The Advanced Research version of the Weather Research and Forecasting model (WRF-ARW; Skamarock et al. 2005), version 2.2, was chosen for this study, and a WRF tracer model was developed, in which an online tracer calculation algorithm is implemented into the model, to study the signal technique and tracer transport.

To simplify the problem, no emission data but signals were released from source points, and the background concentration was set to zero for testing in this study. However, at each source location one constant tracer was released for validation of the signal technique. Imbalances in the model initial fields result in many spurious short waves, mainly gravity waves, during the first few hours of the WRF simulation. To avoid these spurious short waves, the tracers and signals were released into the model 12 h after the initial time. The form of the signals (sig) added to WRF in this study is

$$\text{sig} = A \sin[2\pi N(T - \text{PT})/\text{TT}], \quad (3)$$

where A is the amplitude, N is the frequency in cycles per day (cpd), T is the model integration time in seconds, PT ($=43\,200 \text{ s}$) is the presimulation time (i.e., 12 h), and TT is the total (86 400) seconds in 1 day.

After some experiments, the applicable frequency range for the two case studies is approximately 15–60 cpd. As described earlier, a big enough frequency interval is a prerequisite for signal identification at the receptors, and, therefore, a frequency interval of around 10 cpd is employed. The amplitude employed for the idealized case study is 50 units per second. For real cases with a signal superimposed onto emission data (although no emission is considered for now), the amplitude of the signal should be much smaller than the real emission and thus a much smaller amplitude (0.0018 units per second) than that used in the idealized case is applied to the semireal case study. The same amplitude is applied for the constant tracers in both case studies.

c. The Weather Research and Forecasting tracer model

A tracer model was developed based on the WRF model (Skamarock et al. 2005). WRF is a next-generation

mesoscale meteorological model that has been robustly tested for both idealized studies and real data simulations/forecasts (Hong et al. 2004; Miglietta and Rotunno 2005; Nolan et al. 2007; Chen et al. 2008b, and others). WRF is a fully compressible, 3D nonhydrostatic model, and its governing equations are written in flux form to conserve mass and dry entropy. WRF is well designed and modularized, so that it is relatively easy to develop an online tracer model within the WRF model framework by adding four-dimensional tracer variables to the model. In this online tracer model, the transport of tracers is treated as a modeled scalar, and the effects due to advection and eddy mixing are taken into account in the tracer calculation. The only source term for tracers is the emission from the surface injected into the first half-model level. To apply the signal technique in this WRF tracer model, the tracers are replaced with signals because no emissions are considered in this study.

d. Time series analysis tools

Time series data often contain different time scales of frequencies. These frequencies are in general difficult to see from original data directly (Priestley 1981). Many numerical tools, such as FT or wavelet analysis (WA), can transform data from a physical space into a frequency domain. During air-pollution episodes, receptors have pollutants that are contributed from both local and non-local emissions. In addition to knowing where the pollutants are coming from, the arrival time from each source can help to identify the problem more precisely and is important for emission control. Therefore, both source locations and arrival times are of interest in our spectral analysis for this source–receptor study. Unlike FT, short-time Fourier transform (STFT) and WA can provide additional, though rough, information about the timing of those signals. Although wavelet decomposition could provide decent time and frequency information both, a proper STFT can present much higher frequency resolution (Bentley and McDonnell 1994). Therefore, in addition to FT, STFT is applied to the time series analysis in this study.

A conceptual diagram of the STFT is shown in Fig. 1. The time series to be analyzed (Fig. 1a) is composed of sinusoidal functions, with the frequency changing from hour to hour. For hours 1, 2, and 3, the frequencies are 10 cycles per hour (cph), 15 cph, and 20 cph, respectively. First, time series data are divided into different segments in sequence. For the given example, we intend to see the frequency changes; thus, 1-h segments of data are used. Second, a window function, which is nonzero only for the data segment of interest, is chosen. Commonly used windows include rectangular, Hann, or Gaussian, with the rectangular window function being the choice

in this study (Fig. 1b). Third, the time series data are multiplied by the window function to produce a new time series (Fig. 1c). Last, FT is applied to the new time series to analyze the frequency in that particular time period (i.e., the information of occurring time). Figure 1d shows the spectra for the first hour of the example time series. The procedure is repeated from the first to the last segment by sliding the window a half segment each time to avoid losing frequency information between the time segments. Therefore, a total of five data series would be analyzed for this example. The length of the window is important. A shorter (longer) time window results in better (worse) resolution in time (i.e., a more precise occurrence time) but worse (better) resolution in frequency (Kaiser 1997). The window length chosen for the semireal case study was mainly based on the duration of the highly polluted periods.

3. Idealized-case experiment

a. Model configuration

To explore the applicable frequencies and the appropriate frequency intervals between signals, as well as to investigate the use of the signal technique within the WRF framework, an idealized 3D simulation was first conducted. The WRF idealized supercell case was chosen for this purpose. A single model domain of 100×100 grid points with 2-km horizontal spacing was configured. There were 41 stretched layers in the vertical direction, with a model top of 20 km. The 1.5-order prognostic turbulence kinetic energy (TKE) subgrid-scale eddy diffusion and Purdue–Lin microphysics (Chen and Sun 2002) were applied. The time step was 10 s, and the model integrated for 1.5 days.

b. Selection of source and receptor locations

Proper evaluation of the signal techniques requires that the idealized numerical experiments be designed carefully. For example, sources must be located where they are sure to have some impact on the receptors. The winds fields from a preliminary idealized supercell run were used to guide the placement of the tracer sources. It was found that the supercell moved out of the domain after 3–4 h of integration, leaving behind perturbed mean winds propagating within the domain. Because tracer transport is determined mostly by the low-level wind field and the pathways are generally aligned with the wind direction, source placement can be guided by plots of a low-level wind field. A snapshot of the winds at the lowest model level after 12 h of integration (the time when tracers and signals were released) is shown in Fig. 2. Based on this wind field and the fact that the

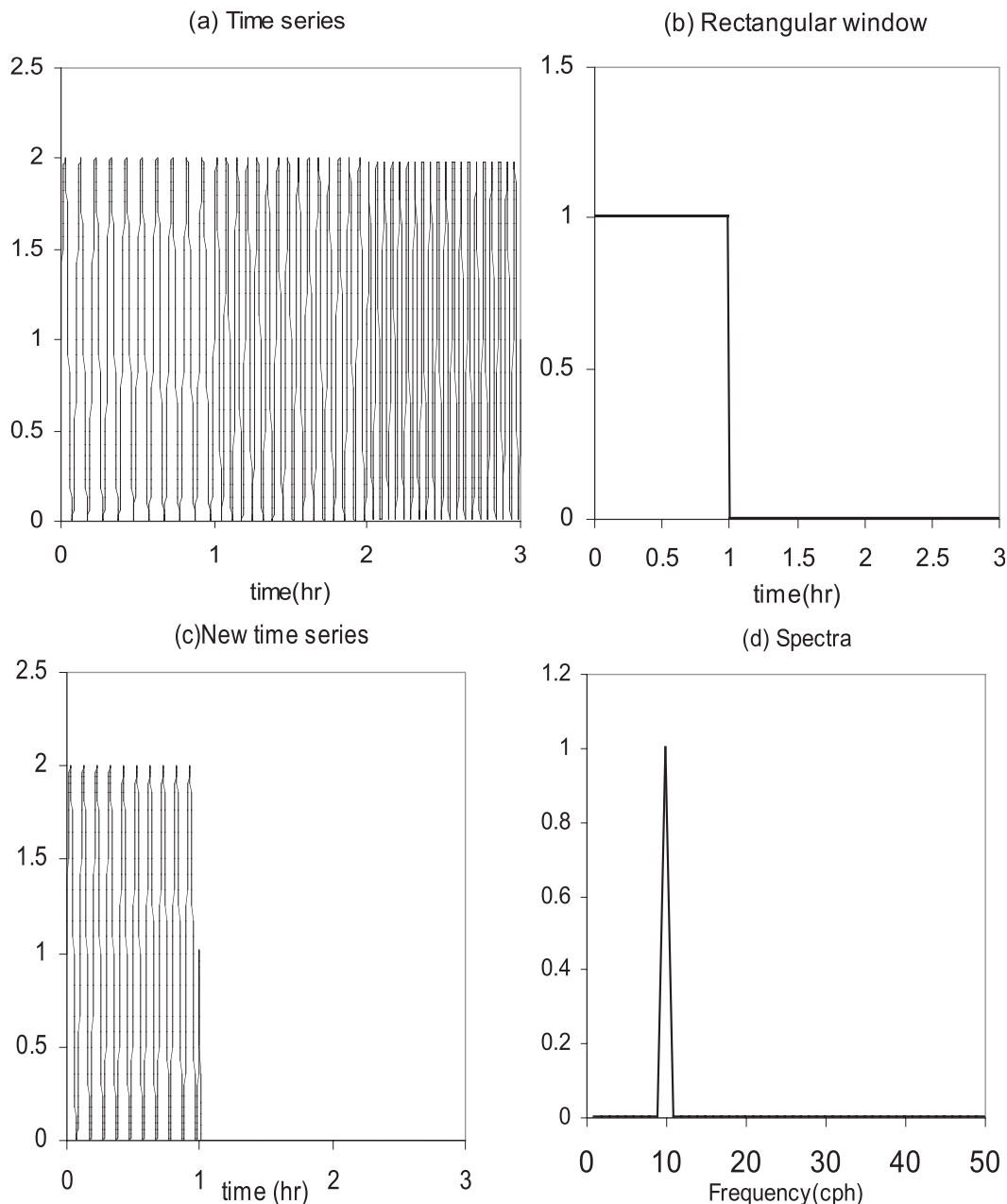


FIG. 1. A conceptual model of STFT. (a) The example time series. (b) The rectangular window. (c) The new series generated by multiplying the time series in (a) by the window function in (b). (d) The spectra for the first segment of the example time series. Note that the y axis in (d) is spectrum.

source points have to be located upstream of the receptors, four sources (s1–s4) were selected (Fig. 2).

c. Idealized-case numerical simulation

The idealized WRF case was run again with the four sources (s1–s4; see Fig. 2) emitting signals and tracers into the lowest model layer. Each source emitted two tracers. The first was a constant tracer of 50 units per

second (designated T1–T4, corresponding to sources 1–4, respectively). The second tracer emitted from each site was T5. This tracer contained a unique oscillatory signal for each site [Eq. (3)] with an amplitude of 50 units per second. From the preliminary run's wind pattern at hour 12 (Fig. 2), it can be estimated that s1 was the source point farthest from the receptors (with s4 being the closest source). To compensate for the dependence of diffusion on distance and frequency, the signal

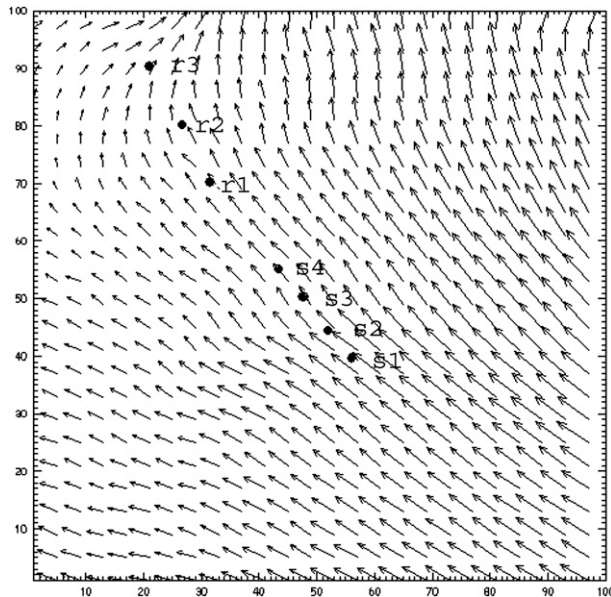


FIG. 2. The simulated wind field at the first half-model-level 12-h integrations. Four source locations (represented by a leading “s”) and three receptors (represented by a leading “r”) were chosen for the source–receptor experiment. The coordinates for the sources and receptors are s1: (55, 40), s2: (50, 45), s3: (45, 50), s4: (40, 55), r1: (30, 70), r2: (25, 80), and r3: (20, 90). The x and y axes are the horizontal grid cells in the model domain.

emitted from the farthest (closest) source point should have the lowest (highest) frequency. Therefore, the frequencies N chosen for the T5 signal were 21, 31, 39, and 47 cpd for sources s1–s4, respectively. The tracer concentrations were saved every minute so as to have detailed time series for spectral analysis.

The frequency spectrum of the T5 concentration time series will be analyzed at the chosen receptors and compared with the constant tracer concentrations (i.e., T1–T4). If the corresponding frequencies of the signals are distinguishable from the spectrum, it implies that the signal technique could potentially achieve the goal of obtaining the source–receptor relationships with better efficiency than the tracer method.

d. Results

After analyzing the 24-h transport pathways of T1–T4 within the whole domain, r1 (30, 70), r2 (25, 80), and r3 (20, 90), which received significant amounts of tracers, were chosen as the receptors (Fig. 2). The distances between the sources and receptors are listed in Table 1. The 1-day evolution of the concentration of the four tracers at each receptor is shown in Fig. 3. Note that the starting point of the x axis in Fig. 3 is the tracer release time (i.e., 12 h after the model initial time) instead of the model initial time. Because a signal and a tracer were

TABLE 1. Distance (km) between the sources and receptors for the idealized case study. Grid coordinates are shown in parentheses.

	s1 (55, 40)	s2 (50, 45)	s3 (45, 50)	s4 (40, 55)
r1 (30, 70)	78	64	50	36
r2 (25, 80)	100	86	72	58
r3 (20, 90)	122	108	94	81

released simultaneously from each source, a receptor that receives a tracer should ideally receive a corresponding T5 signal, assuming that the T5 signal was not completely damped out or aliased. In this case study, every receptor received all four tracers during some period of time (Fig. 3). Thus, the numerical setup here is good for examining whether the signals are still distinguishable at the receptors. Note that the negative tracer concentrations are an artifact of the advection scheme used in WRF. However, the spurious waves due to this problem are much shorter than the real waves because of the strong winds present in this study. Therefore, these artifacts will not have a significant impact on our results and can be eliminated by using the more computationally expensive positive-definite advection scheme available in WRF.

The FT power spectrum for the T5 concentrations at the three receptors (Fig. 4) shows evidence of the retrieved signals. The four primary peaks at r1 obviously correspond to sig1–sig4, respectively (Fig. 4a). This is consistent with the concentration time series plots for the constant tracers (Fig. 3a), which indicate that all four constant tracers were transported to r1 during some period of the simulation. There is a small frequency shift (from 21 to 22 cpd) for sig1 emitted from s1 at r1 (Table 2). In addition to the primary frequencies, a nonnegligible beat frequency exists at 44 cpd, which might be due to the nonlinear interaction between the signals and the nonconstant wind field. At r2, the signal emitted from s2 (sig2; 31 cpd) was in the process of shifting to a higher frequency (32 cpd; see Fig. 4b) while the amplitude for frequency 48 cpd, which corresponds to sig4, is much smaller than the other three primary peaks. At r3, the farthest receptor (Fig. 4c), the spectrum has three clear peaks at frequencies 22, 32, and 40 cpd (Table 2). In this idealized case, all frequency shifts appear to be in one direction (i.e., shifting to higher frequency), and at r3 all of the signals were shifted to slightly higher frequencies (Table 2). Because these shifts are sufficiently smaller than the intervals between two successive signals, the signals are still distinguishable. The magnitude of T4 was too small relative to the other constant tracers at r2 and r3 (Figs. 3b and 3c) and, therefore, almost could not be detected in the spectrum analysis. A comparison of the three FT spectrum

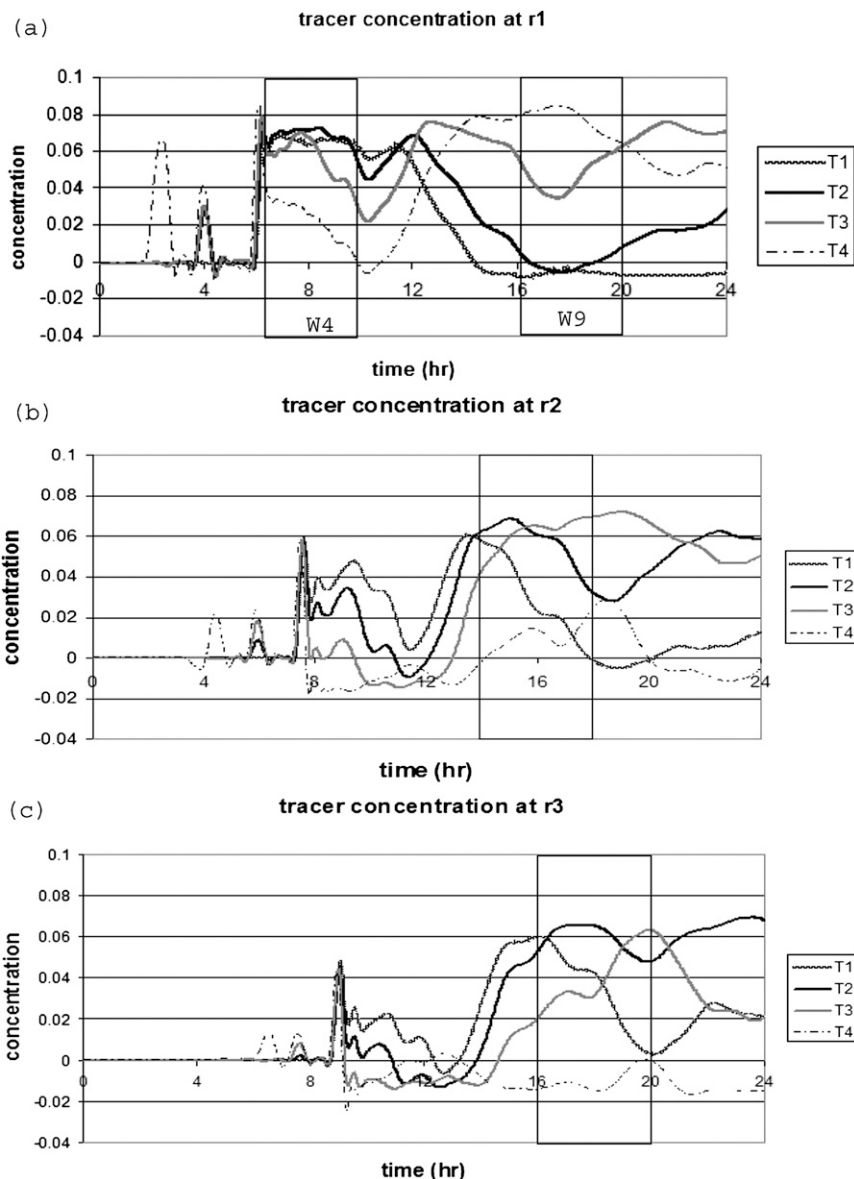


FIG. 3. Time evolution of the concentration of T1–T4 received at (a) r1, (b) r2, and (c) r3. The rectangular encompassed areas in (a) are the time windows for STFT analysis in Fig. 5; W4 spans hours 6–10 and W9 spans hours 16–20 at r1. The time window in r2 spans hours 14–18, and that in r3 spans hours 16–20.

plots in Fig. 4 shows that the signal amplitudes get smaller as the distance between the source and receptor increases because of the fact that 1) lower amounts of tracers reached the farther receptors, as demonstrated in Fig. 3, and 2) the damping of the signal amplitude by diffusion is related to the transport distance. Despite the slight shift in frequency, the signals retrieved from FT at all three receptors are consistent with tracer simulations. The main sources contributing to the receptors are identified (s1–s4 for r1, and s1–s3 for r2 and r3) from the FT results. The biggest distance

between the source and receptor (from s1 to r3) is about 122 km, and the signals are still clearly shown at the receptors. This implies that the signal technique can potentially be applied to 3D regional real-data case studies.

Next, the simulation results were analyzed using STFT to get the frequency information for different time segments. As mentioned before, choosing an appropriate time window length is very important for STFT analysis. After testing several different window lengths, a 4-h time window was selected to avoid losing too much frequency

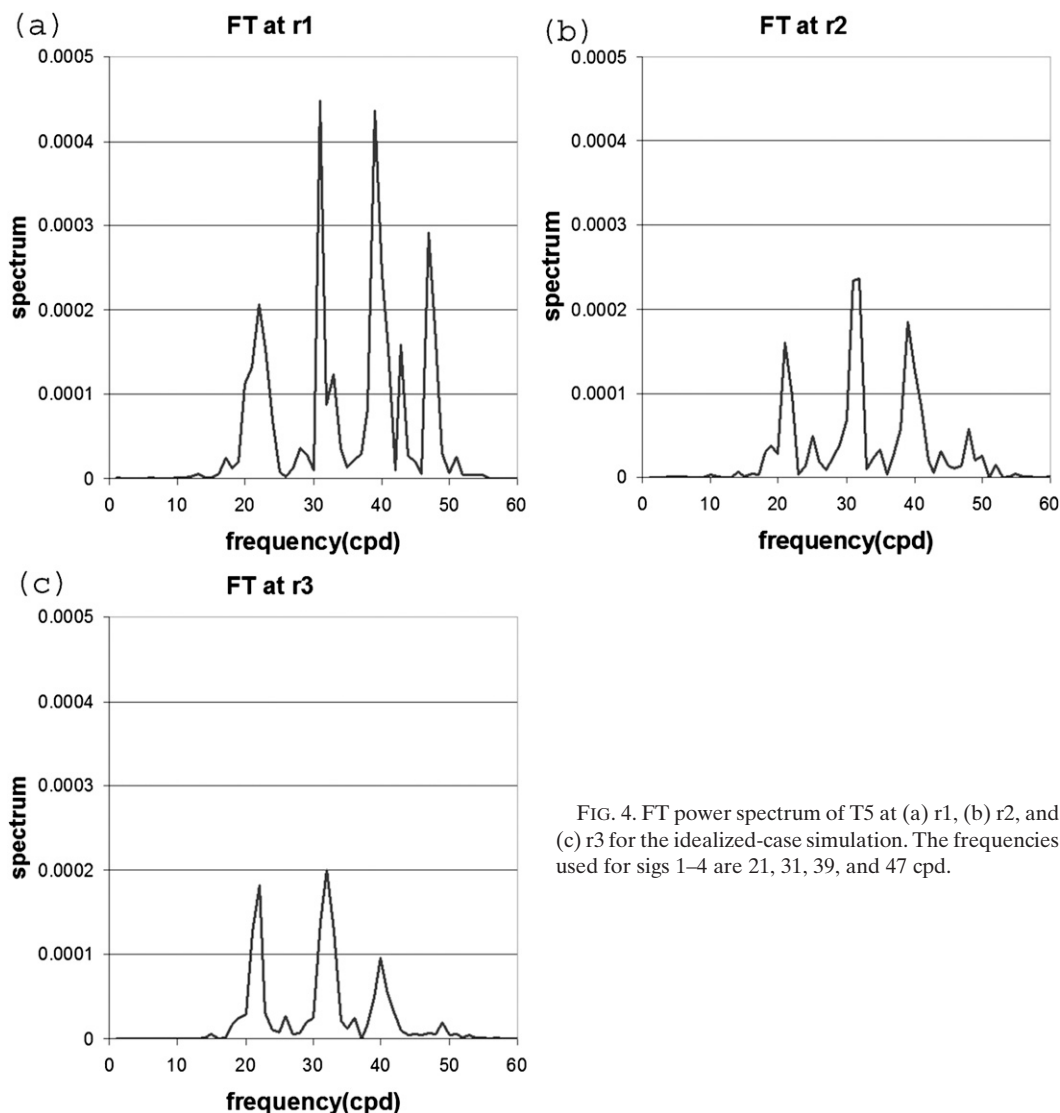


FIG. 4. FT power spectrum of T5 at (a) r1, (b) r2, and (c) r3 for the idealized-case simulation. The frequencies used for sigs 1–4 are 21, 31, 39, and 47 cpd.

information. Half-overlapping between two segments was applied; thus, there were 11 windows for the 1-day time period. Figure 5 shows the STFT power spectrum for T5 concentration at the receptors, and the matching time windows are depicted in Fig. 3. The power spectrum of W4 (Fig. 5a) has three obvious peaks at frequencies 23, 33, and 42 cpd, corresponding to signals released from s1 to s3, respectively. There is an obscure bulge to the right of the 42-cpd peak, which is very likely from sig4. It is not well resolved because of the relatively poor frequency resolution of the STFT. The STFT frequency shifts are larger than those in the FT analysis. Window W9 has two peaks at frequencies of 39 and 48 cpd, which correspond to signals released from s3 and s4, respectively. The results of the simulated tracers received at r1 illustrate that within the W4 time window the concentration of T4 was

much smaller than those from the other three sources whereas for W9 the concentrations of T1 and T2 are almost negligible in comparison with those of T3 and T4 (Fig. 3a). The STFT spectra at r2 (Fig. 5c) and r3 (Fig. 5d)

TABLE 2. Retrieved signals (cpd) from FT analysis at the receptors for the idealized-case simulation. The frequency-shift directions (H: shifting to higher frequency; L: shifting to lower frequency; U: frequency unchanged) are specified in parentheses following the frequency. “None” indicates the corresponding frequency is not in the spectrum.

	sig1 (21)	sig2 (31)	sig3 (39)	sig4 (47)
R1	22 (H)	31 (U)	39 (U)	47 (U)
R2	21 (U)	31–32 (H)	39 (U)	48 (H)
R3	22 (H)	32 (H)	40 (H)	None

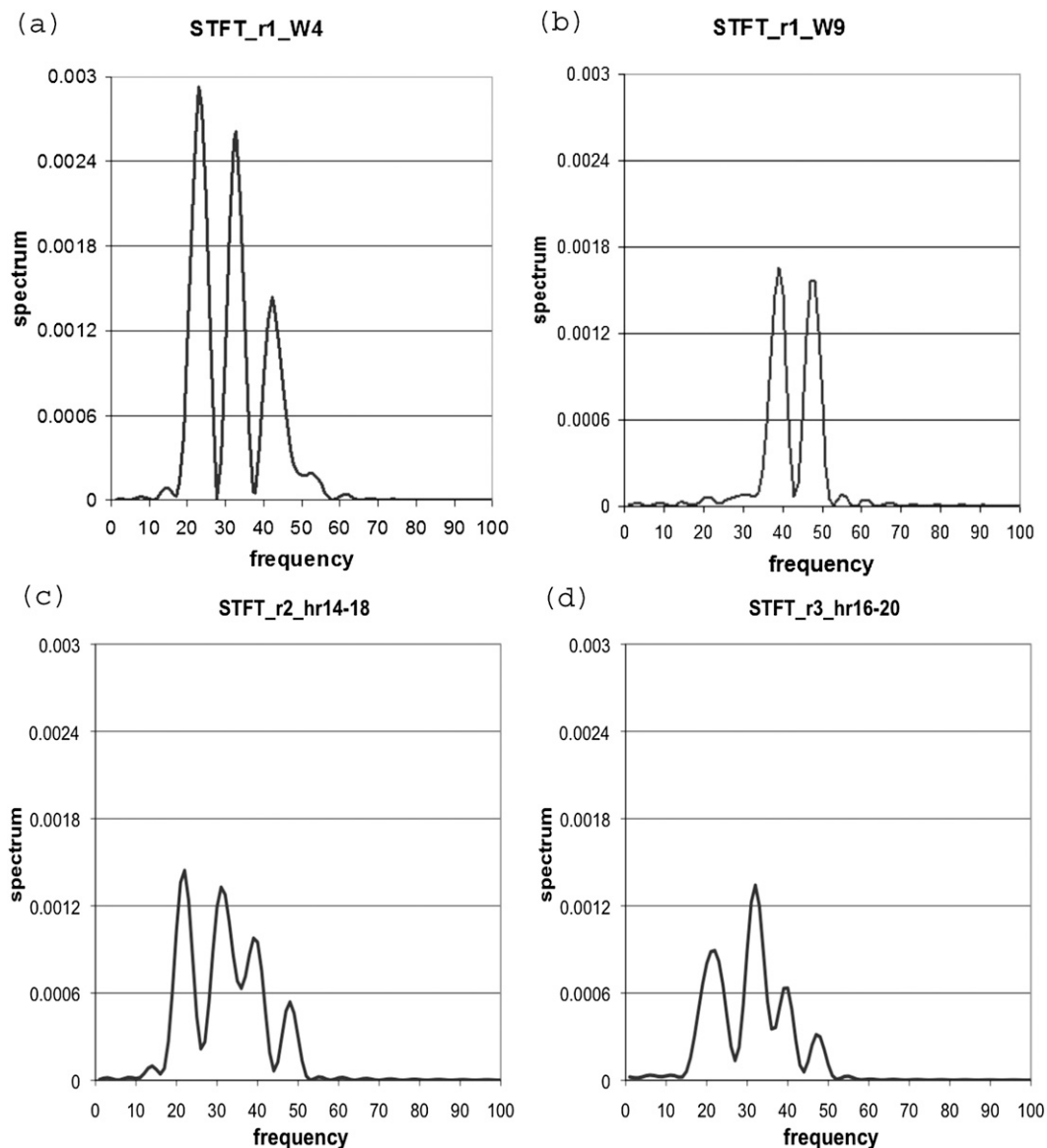


FIG. 5. STFT spectrum for (a) W4 and (b) W9 at receptor r1, (c) hours 14–18 at r2 and (d) hours 16–20 at r3. The time windows for these STFT are shown in Fig. 3.

indicate that the tracers from all four sources contributed to these receptors during the analysis time period, which is consistent with the constant tracer results (Figs. 3b and 3c). However, the peaks of the spectrums at r2 and r3 are less sharp with smaller amplitudes as compared with those at r1 because of the longer transport. The STFT spectrum has much less noise as compared with the FT analysis (Fig. 4), and no evidence of secondary frequencies (i.e., beat signal) exists in any of the STFT results. However, the STFT-retrieved frequencies are broader (i.e., less precise) than the FT results and the frequency shifts seem to be more severe, both of which are likely due to the lower resolution in frequency as compared

with FT. Therefore, to use STFT, relatively bigger frequency intervals between signals are required.

e. Frequency diffusion sensitivity test

In this experiment, five tracers (T1–T5) were emitted from the same source point, s1 in Fig. 2, with each of them carrying one unique oscillatory signal (i.e., a unique frequency). The frequencies used for T1–T5 were 21, 31, 39, 47, and 59 cpd, respectively. Otherwise, the numerical experiment setup was identical to the previous experiment. Hsu and Chang (1987) pointed out that the diffusion effect depends on the signal frequency and the distance between the source and receptor. Because all of

the tracers were emitted from the same location (s1), the distance between the source and each receptor is the same for all of the tracers (i.e., T1–T5). The diffusion effect with respect to the signal amplitude modulation of different frequencies in 3D simulations can be studied. The time series of tracer concentration were analyzed at the three receptors using FT. The relationship between the frequency and the damping effect is evident from the power spectra of all five tracers at the receptors (Fig. 6 and Table 3). The frequencies at 21, 31, 39 and 47 cpd were still detectable at all three receptors, and the amplitudes decreased as the frequencies increased. The frequency modulation of the amplitude is demonstrated well from this experiment, which indicates that frequencies higher than 55 cpd might not be applicable for the distance of about 80 km in this case study. The frequency shift is also reflected in Table 3, and it is interesting to see that no shift occurred to all of the retrieved signals at the farthest receptor (r3), but some nonnegligible beat frequencies appear at r3 (Fig. 6c) after the relatively longer transport. This experiment demonstrates that the diffusion effect on amplitude damping is stronger for higher frequencies than for lower frequencies in this 3D supercell simulation, which is consistent with the 2D simulation results in Hsu and Chang (1987).

4. Semireal-case experiment

We would like to investigate the feasibility of the signal approach applied to real-world cases. However, there are some practical limitations that must be considered. Chen and Hsu (2006) demonstrated that signals were preserved better with the use of a 1.5-order prognostic TKE scheme or Smagorinsky subgrid-scale eddy diffusion (SGED) than with the use of the K -theory diffusion scheme. Both of the SGED schemes are not recommended for cases with horizontal resolution coarser than 2 km (recommended in the WRF model). Such fine resolution requires great computational resources to conduct the simulation, which negates the advantage of the signal approach—namely, reducing computational demand by employing fewer tracers. This is an internal limitation of the signal approach when applied to real case studies. Because of the great computational demand to conduct the simulation and the limitation of available computational resources, the chosen case study's analysis domain only covers a small region, with the pollutant transport distance on the order of 1000 km. As a result, instead of solving real source–receptor relationships for an air-pollution event, this case study is used to demonstrate the signal technique under real atmospheric conditions with synthetic sources and receptors

not necessarily located in large cities where high pollution amounts are typically observed. Therefore, this case study is called a semireal case study.

a. Case selection

High-pollution episodes occurred in Istanbul, Turkey, from 5 to 12 January 2002 (Kindap et al. 2006). During that time period, an anticyclone located over central Europe resulted in strong winds and favorable conditions for pollutant transport from upstream of Istanbul. Previous studies (Kindap et al. 2006; Chen et al. 2008a) proved that pollutants from upstream were transported to Istanbul by northwesterly low-level flow and played a nonnegligible role in this event. The episode from 0000 UTC 5 January to 0000 UTC 8 January 2002 was selected to examine the feasibility of applying the signal technique in a 3D semireal case simulation to solve the source–receptor relationships.

b. Model configuration

In this experiment, three nested domains (Fig. 7) were configured with horizontal spatial resolutions of 30, 10, and 2 km for domains 1–3 (d1–d3), respectively. All three domains have 31 vertically stretched layers. Six-hourly forecast outputs from the National Centers for Environmental Prediction's Global Forecast System (GFS) model, with a spatial resolution of $1^\circ \times 1^\circ$, were used to provide the initial and boundary conditions. Domains 1 and 2 were first integrated with two-way interaction for all 3 days, from 0000 UTC 5 January to 0000 UTC 8 January 2002. During the integration, d1 was nudged with the GFS reanalysis using four-dimensional data assimilation to maintain large-scale features. Results from d2 were one-way nested down to provide boundary conditions for the d3 simulation, which was used to examine the signal technique. Time steps of 90, 30, and 10 s were used for d1–d3, respectively. The signal and tracer simulation was only performed in d3.

The Mellor–Yamada–Janjić TKE boundary layer scheme (Mellor and Yamada 1982; Janjić 2002) and the Kain–Fritsch cumulus parameterization scheme (Kain and Fritsch 1993) were applied to d1 and d2. Thompson microphysics, Dudhia shortwave radiation and Rapid Radiative Transfer Model longwave radiation were used for all three domains. Because of the fine spatial resolution, no cumulus scheme was applied to d3. As mentioned previously, the signal approach has been shown to work better with the SGED scheme; so, to be consistent with the idealized case, the 1.5-order prognostic TKE SGED was applied to this case study. Because of the fine-resolution requirement of the TKE SGED scheme (≤ 2 km), it was applied to the d3 simulation only. As in the idealized study, tracers and signals were

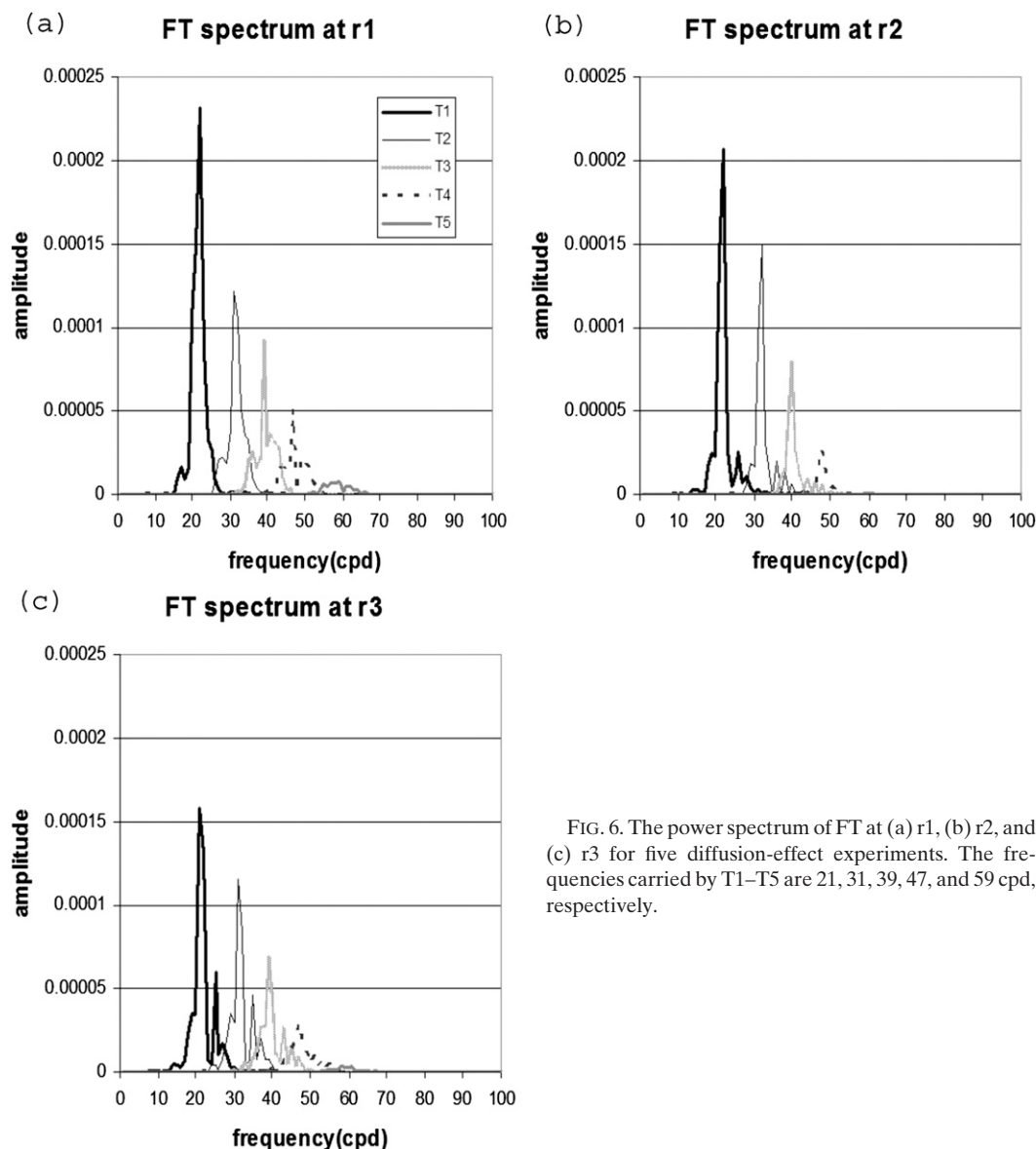


FIG. 6. The power spectrum of FT at (a) r1, (b) r2, and (c) r3 for five diffusion-effect experiments. The frequencies carried by T1–T5 are 21, 31, 39, 47, and 59 cpd, respectively.

emitted 12 h after the initial time in the d3 simulation. The concentrations of the tracers and signals were saved every minute for spectrum analysis.

c. Selection of sources and receptors and numerical experiment design

The simulated wind field and sea surface pressure (Fig. 7) from d1 illustrated that the simulation captured the anticyclone circulation described in Chen et al. (2008a), which assured strong winds (i.e., efficient transport) in the d3 simulation. The selection of the source and receptor locations in the real atmosphere was more difficult than in the idealized case since the change in wind patterns was more dramatic. Chen et al. (2008a)

demonstrated that, because of the strong static stability during the event, pollutants that were transported downstream were mainly trapped within 1.2 km depth from the surface. Therefore, low-level winds were used for reference to select source and receptor locations, and

TABLE 3. Retrieved signals (cpd) from FT analysis at the receptors for the sensitivity test. The amplitudes (order of 10^{-4}) for the corresponding frequencies are specified in the parentheses in the data rows.

	sig1 (21)	sig2 (31)	sig3 (39)	sig4 (47)	sig5 (59)
r1	22 (2.31)	31 (1.22)	39 (0.92)	47 (0.51)	None
r2	22 (2.07)	32 (1.49)	40 (0.79)	48 (0.27)	None
r3	21 (1.58)	31 (1.15)	39 (0.68)	47 (0.29)	None

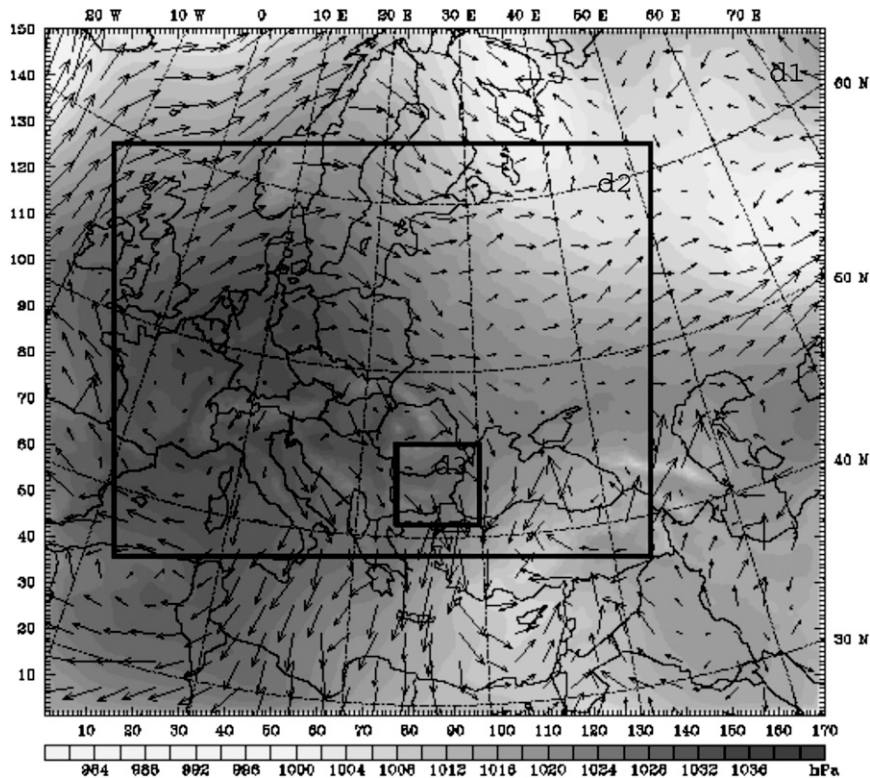


FIG. 7. Nested domains for the semireal-case simulation with sea level pressure (shaded; hPa) and surface wind vectors at 1200 UTC 5 Jan 2002.

time series data collected at the first model level were used for spectrum analysis.

As mentioned previously, the source and receptors in this case study are not necessarily in the big cities. To choose appropriate source and receptor points, dozens of constant tracers were emitted from upstream of the Istanbul area based on the lowest-level wind field. From the pathways of those tracers, three source points (s1–s3) were selected (Fig. 8). Frequencies of 15, 21, and 27 cpd were chosen for signals emitted from s1, s2, and s3, respectively. All three signals used the same amplitude (0.0018 units per second), and they were summed and saved in tracer 4 (i.e., T4). Tracers T1–T3 with the same emission rate were released from sources s1–s3, respectively, for validation of the signal technique, as in the idealized case. To be consistent with the signals, the emission rate of 0.0018 units per second is applied to all three constant tracers.

d. Results

Two receptors downstream of s1–s3 were chosen (Fig. 8). The distances between the sources and receptors, as well as the coordinates for each of them, are shown in Table 4. The time evolution of tracer concentrations for T1–T3 at both receptors is illustrated in Fig. 9 for the time

periods when the tracers passed the receptors. Relative to r2, r1 is closer to the sources, and therefore T1 and T2 arrived at r1 several hours earlier than they arrived at r2. About 37 h after the initial time, all three tracers reached r2, and they continuously passed there for about 14 h. A 12-h time window STFT was used to decompose the T4 (with signals) concentration so as to include the major time periods during which the receptors continuously received the tracers. Therefore, the window covers different time segments for r1 (hours 36–48) and r2 (hours 38–50) (Fig. 9). The spectrum for r1 within the 12-h time window (Fig. 10a) has two distinct peaks at 15 and 21 cpd, which correspond to the signals emitted from s1 and s2, respectively. This is consistent with the tracer concentration plot at r1 in Fig. 9a, which showed that only T1 and T2 were received by r1 during the analysis time window. For the spectrum at r2, three primary peaks were obtained at 14, 20, and 27 cpd, corresponding to signals from s1, s2, and s3, respectively. As in the idealized case, there was a secondary peak (i.e., beat) at 23 cpd due to the nonlinear effect in the numerical simulation. It is noticed again that signals from s1 and s2 were shifted slightly to lower frequencies when received at r2. Note that the shift direction here is different from the idealized case in which the frequencies were shifted higher. The frequency shifts

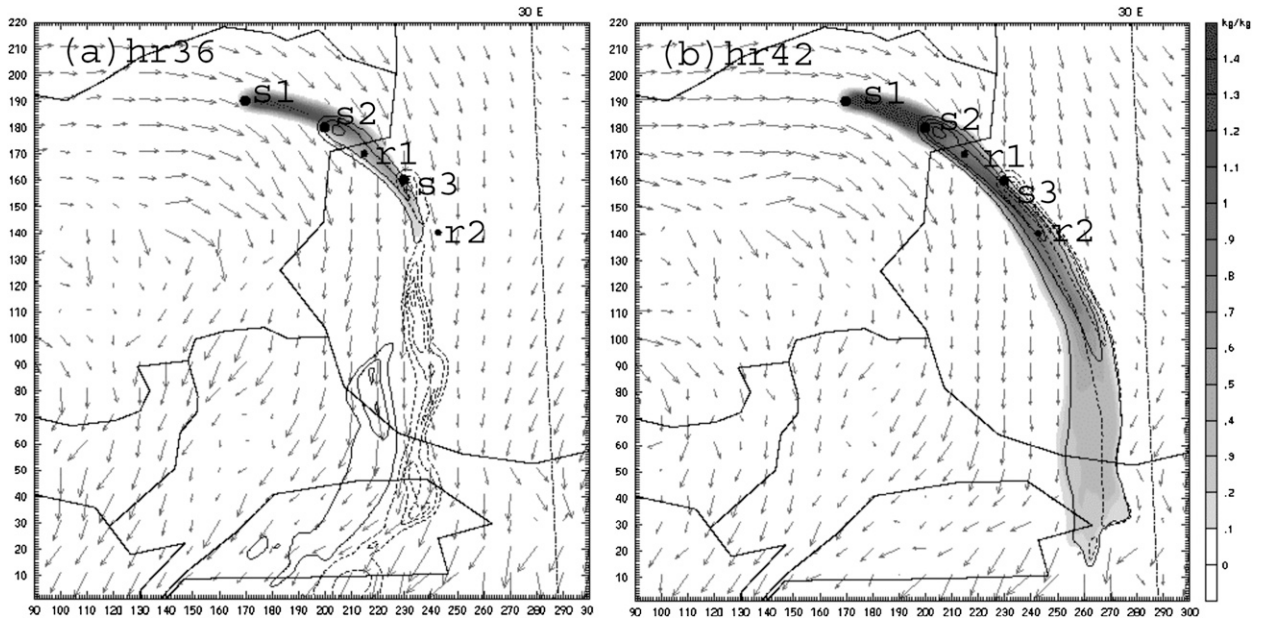


FIG. 8. Snapshots of simulated constant tracers on the first level and wind vectors at 950 hPa after (a) 36 and (b) 42 h of simulation. Here, T1 (shaded) is released from s1, T2 (solid lines) is released from s2, and T3 (dashed lines) is released from s3. The x and y axes are the grids in the east–west and south–north directions of domain 3. The two receptors are denoted as r1 and r2. Note that r1 is upwind of s3.

(which require a certain amount of time and/or transport distance to manifest themselves) occur in both the idealized and semireal cases.

Figure 11 shows the time-averaged tracer amounts of T1–3 received at r1 and r2 over the aforementioned 12-h period. Because of the setup of this case study (i.e., r1 is upwind of s3), T3 is not received at r1. At r1, more T2 is received than T1 (Fig. 11) and the spectrum for sig2 is larger than for sig1 (Fig. 10a), indicating that the two components of the diffusion effect (distance and frequency) counteract each other, with the spectrum reflecting the relative source contribution, to some degree, for this case. At r2, the amounts of T1 (sig1) and T2 (sig2) received were very similar to those received at r1 (Figs. 10b and 11). However, because the relative distances between the source points s1 and s2 are smaller for r2 than for r1, there was a stronger damping effect on the higher-frequency signal (sig2) than the lower-frequency signal (sig1) at r2 (Fig. 10). However, the sig2 received at r2 was still slightly larger than the sig1 because the amount of tracer received was slightly larger (Fig. 11). With similar amounts of T1 received at r1 and r2, although the transport distance to r2 is longer than to r1, the retrieved sig1 spectrum at r2 is stronger than at r1. One possible reason for this result is that the spectrum band for sig1 is sharper at r2 than at r1. The more the spectrum band spreads, the greater is the reduction in the magnitude. Despite the fact that more T1 was received

at r2 than T3, the spectrum values for these two signals were almost the same in Fig. 10b. This is because the signal from s1 was diffused more because of a much longer transport distance (~180 km) than the signal from s3 (~50 km), even though sig3 has a higher frequency (i.e., more diffuse) than sig1. This implies that the difference in transport distance dominated the signal-damping effect rather than the differences in frequency for this particular situation (i.e., T1 and T3 received at r2). Therefore, spectrum analysis can reflect the significance of the emission source to some degree but not the amount because the damping rate on a signal’s amplitude is not only influenced by the transport distance but is also affected by the frequency, yet there is no clear correlation between these two factors (i.e., distance and frequency).

A shorter time window (6 h) was also applied to the T4 concentration time series received at r2. The two periods are hours 38–44 (W1) and 44–50 (W2), which are equivalent to the first and second halves of the

TABLE 4. As in Table 1, but for the semireal case study. Note that no tracers from s3 are transported to r1 because r1 is upwind of s3.

	s1 (170, 190)	s2 (200, 180)	s3 (230, 160)
r1 (215, 170)	98	36	—
r2 (243, 140)	177	117	48

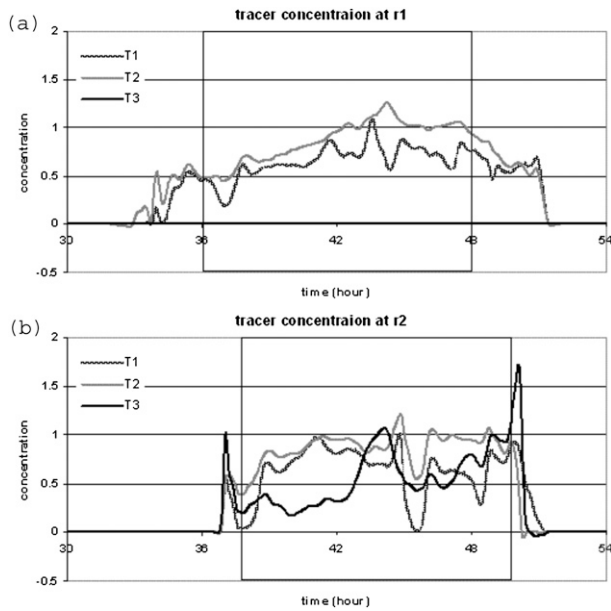


FIG. 9. Concentration time series plots of T1–T3 at (a) r1 and (b) r2. The two rectangular encompassed areas are the 12-h window coverage for STFT analysis. Note that there is no T3 at r1 because s2 was located downstream of r1.

previously used 12-h time window at r2. The three peaks are 13, 19, and 27 cpd for W1 (Fig. 12a), and 14, 22, and 27 cpd for W2 (Fig. 12b). It is interesting that there are no apparent 23-cpd beat signals similar to the ones in the 12-h window analysis in Fig. 10b. However, the retrieved signal spectrums were wider (i.e., less precise) than the

12-h window results, indicating that a higher resolution in time was obtained (i.e., 6- vs 12-h time resolution) at the cost of losing accuracy in signal frequency. It is noticed that the amplitudes of sig1 and sig2 are much bigger than that of sig3 in the W1 spectrum (Fig. 12a), despite the shorter distance between s3 and r2. For most of the time within W1, the concentration of T1 and T2 is more than 2 times that of the T3 concentration at r2 (Fig. 9b). The higher amplitudes may also be related to the frequency shifts of sig1 and sig2 to lower frequencies by 2 cpd, which in theory would lead to less of a diffusion damping effect. In the W2 results (Fig. 12b), the signal from s1 is damped out the most. In addition to a longer distance, this damping might be related to the less continuous concentration of T1 at r2 (Fig. 9b) so that not many full cycles of sig1 were received (i.e., broken signal cycles, as sig1 has the lowest frequency). Although there are some unresolved issues, the STFT results, from both the 12- and 6-h windows, captured the three signals that were supposed to be received at the receptors, and the spectrum values could moderately represent the relative source contribution, but not the exact fraction. The results are consistent with tracer simulations.

5. Conclusions and future work

An online tracer model was developed by implementing a tracer conservation equation into the WRF model. In theory, the online approach should better simulate the source–receptor relationships because it avoids the main sources of error in the offline approach. One major

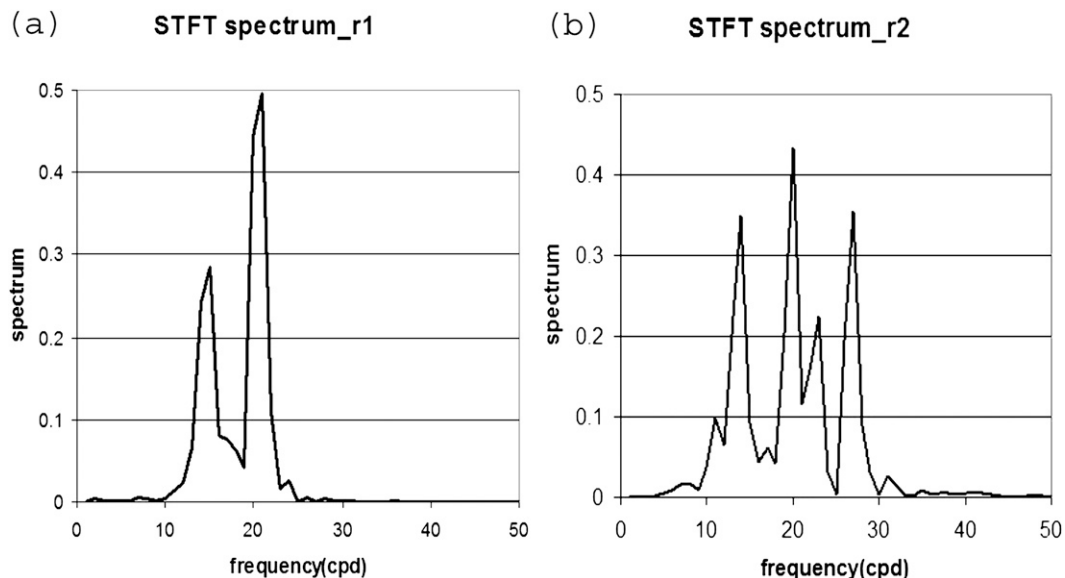


FIG. 10. The 12-h STFT spectrum plots for (a) r1 and (b) r2 from the rectangular time periods in Figs. 9a and 9b, respectively. The frequencies carried in the tracer are 15, 21, and 27 cpd. Note that there is no sig3 at r1 because s3 was located downstream of r1.

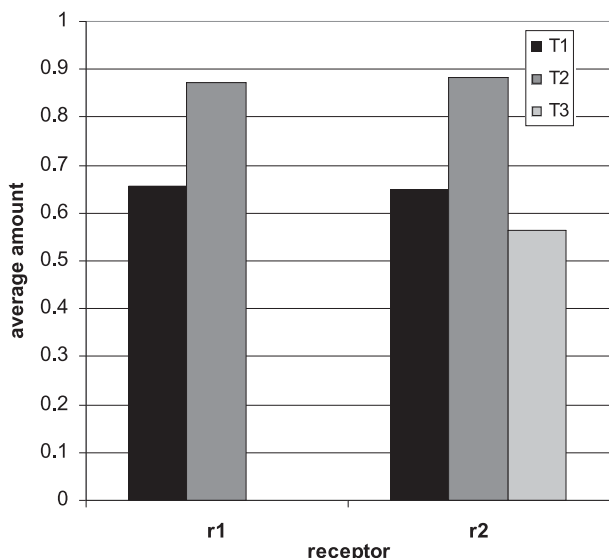


FIG. 11. Averaged tracer amounts at r1 and r2 over the 12-h time period (hours 36–48 for r1 and 38–50 for r2). Note that there is no T3 at r1 because s3 was located downstream of r1.

problem with the online approach is the tremendous computational resources required for a large-airshed simulation. The signal technique could potentially alleviate this problem by using signals of different frequencies instead of many separate tracers to differentiate pollutants emitted from different locations.

The primary goal of this study is to assess the performance of this signal technique in the complex 3D non-hydrostatic online WRF tracer model. The evaluation

was carried out using a 3D idealized supercell case and a semireal air-pollution case. Although the signals were damped by the diffusion effect, the spectrum analysis results from either FT or STFT were consistent with the constant-tracer simulations used to verify the signal technique for both cases. Although only a semireal case is conducted in this study, with enough computer resources this signal technique should be able to solve real air-pollution cases in which the signals are emitted from the potential emission sources (big cities) and spectrum analysis is conducted at the locations of interest. A noticeable frequency shift appeared in some spectrum results as a result of a nonconstant wind, and secondary frequencies (i.e., beats) were obtained because of non-linear effects. With a shorter STFT time window, the spectrum had fewer beat frequencies, but the peak spectrum bands were wider and the frequency shift problem was more apparent. The frequency shift, spread, and beat frequencies due to the nonconstant wind in the real atmosphere will add difficulty for signal identification at the receptors. In addition, all of these internal problems associated with this signal technique are more significant as the transport distance increases; thus, this technique can be only applied to solve medium-range transport within about 1000 km. The frequency dependence of the diffusion effect (too-high frequencies are not usable) and the existing waves in the atmosphere (too-low frequencies are not usable) constrains the suitable frequencies for this signal approach to a relatively small range. One way to solve this problem is to use smaller frequency intervals, which then requires a more

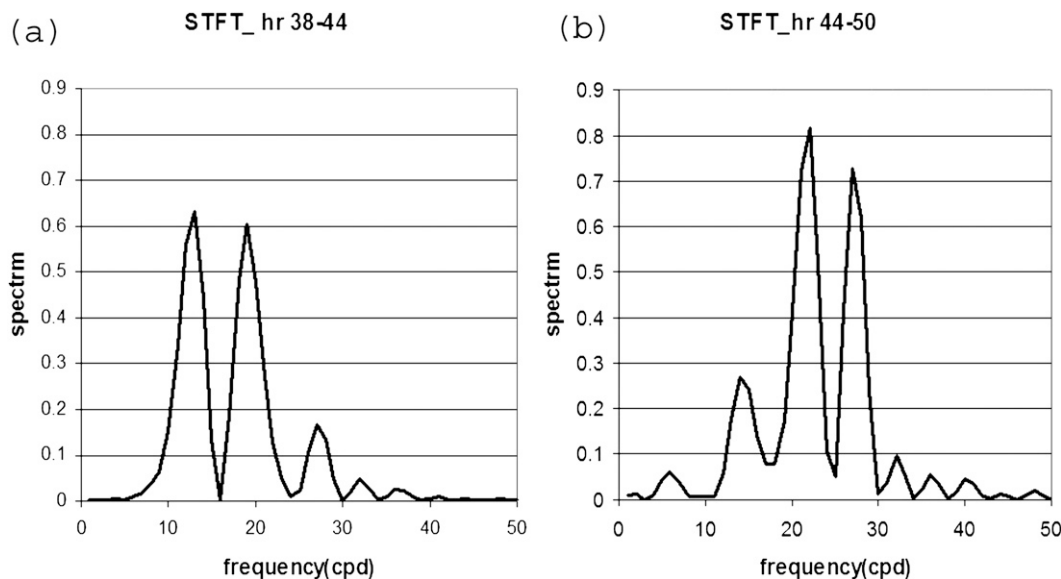


FIG. 12. The 6-h time-window STFT analysis at r2 for the time periods of (a) hours 38–44 (W1) and (b) hours 44–50 (W2).

advanced time series analysis tool to obtain the spectrum. The spectrum could not show the exact contribution fraction because of the damping effects of distance and different frequencies. However, this signal technique might be applied as a screening tool to sort out the important sources in real air-pollution cases. Then, a tracer method could be applied to find the exact source-receptor relationship.

Note that with chemical reactions, which are very important for air-pollution problems, there will be new frequencies generated by interactions between the existing signals. For example, if a secondary pollutant species is formed from the chemical interaction between one species from source A tagged with a signal frequency of f_1 and the other from source B tagged with a signal frequency of f_2 , this secondary species would be associated with the frequency of $|f_1 + f_2|$ and $|f_1 - f_2|$. Signal identification becomes much more complex. This issue needs to be explored in more depth in the future to be able to solve actual air-pollution problems.

Acknowledgments. The authors acknowledge the WRF development teams for their efforts on the model development. We also thank Drs. Hsiao-Ming Hsu and Jim Bresch at NCAR for their helpful discussions on this study.

REFERENCES

- Bentley, P. M., and J. T. E. McDonnell, 1994: Wavelet transforms: An introduction. *IEE Electron. Comm. Eng. J.*, **6**, 175–186.
- Berntsen, T. K., S. Karlsdóttir, and D. A. Jaffe, 1999: Influence of Asian emissions on the composition of air reaching the northwestern United States. *Geophys. Res. Lett.*, **26**, 2171–2174.
- Brunekreef, B., and S. Holgate, 2002: Air pollution and health. *Lancet*, **360**, 1233–1242.
- Chen, S.-H., and W.-Y. Sun, 2002: A one-dimensional time-dependent cloud model. *J. Meteor. Soc. Japan*, **80**, 99–118.
- , and H.-M. Hsu, 2006: The effect of parameterized sub-grid-scale diffusions on the source-receptor relationship in the WRF model. *Geophys. Res. Lett.*, **33**, L18809, doi:10.1029/2006GL026954.
- , J. Dudhia, J. S. Kain, T. Kindap, and E. Tan, 2008a: Development of the on-line MM5 tracer model and its applications to air pollution episodes in Istanbul, Turkey and Sahara dust transport. *J. Geophys. Res.*, **113**, D11203, doi:10.1029/2007JD009244.
- , Y.-L. Lin, and Z. Zhao, 2008b: Effects of unsaturated moist Froude number and orographic aspect ratio on a conditionally unstable flow over a mesoscale mountain. *J. Meteor. Soc. Japan*, **86**, 353–367.
- Dockery, D. W., and C. A. Pope III, 1994: Acute respiratory effects of particulate air pollution. *Annu. Rev. Public Health*, **15**, 107–132.
- EPA, 1996: Air quality criteria for particulate matter, Vol. 1. U.S. Environmental Protection Agency Tech. Rep. EPA/600/P-95/001aF, 1076 pp. [Available online at <http://cfpub.epa.gov/ncea/cfm/recordisplay.cfm?deid=2832>.]
- Fox, D. G., 1981: Judging air quality model performance: A summary of the AMS Workshop on Dispersion Model Performance. *Bull. Amer. Meteor. Soc.*, **62**, 599–609.
- Grell, A. G., S. E. Peckham, R. Schmitz, S. A. McKeen, G. Frost, W. C. Skamarock, and B. Eder, 2005: Fully coupled “online” chemistry within the WRF model. *Atmos. Environ.*, **39**, 6957–6975.
- Held, T., Q. Ying, M. J. Kleeman, J. J. Schauer, and M. P. Fraser, 2005: A comparison of the UCD/CIT air quality model and the CMB source-receptor model for primary airborne particulate matter. *Atmos. Environ.*, **39**, 2281–2297.
- Hong, S.-Y., J. Dudhia, and S.-H. Chen, 2004: A revised approach to ice microphysical processes for the bulk parameterization of clouds and precipitation. *Mon. Wea. Rev.*, **132**, 103–120.
- Hsu, H.-M., and J. S. Chang, 1987: On the Eulerian source-receptor relationship. *J. Atmos. Chem.*, **5**, 103–124.
- Jaffe, D. A., and Coauthors, 1999: Transport of Asian air pollution to North America. *Geophys. Res. Lett.*, **26**, 711–714.
- Janjić, Z. I., 2002: Nonsingular implementation of the Mellor-Yamada 2.5 scheme in the NCEP Meso Model. NCEP Office Note 437, 61 pp.
- Kain, J. S., and J. M. Fritsch, 1993: Convective parameterization for mesoscale models: The Kain-Fritsch scheme. *The Representation of Cumulus Convection in Numerical Models*, Meteor. Monogr., No. 46. Amer. Meteor. Soc., 165–170.
- Kaiser, G., 1997: *A Friendly Guide to Wavelets*. Springer, 324 pp.
- Kindap, T., A. Unal, S.-H. Chen, Y. Hu, M. T. Odman, and M. Karaca, 2006: Long-range aerosol transport from Europe to Istanbul, Turkey. *Atmos. Environ.*, **40**, 3536–3547.
- Kleeman, M. J., L. S. Hughes, J. O. Allen, and G. R. Cass, 1999: Source contributions to the size and composition distribution of atmospheric particles: Southern California in September 1996. *Environ. Sci. Technol.*, **33**, 4331–4341.
- Mellor, G. L., and T. Yamada, 1982: Development of a turbulence closure model for geophysical fluid problems. *Rev. Geophys. Space Phys.*, **20**, 851–875.
- Miglietta, M. M., and R. Rotunno, 2005: Simulations of moist nearly neutral flow over a ridge. *J. Atmos. Sci.*, **62**, 1410–1427.
- Nolan, D., C. Zhang, and S.-H. Chen, 2007: Dynamics of the shallow meridional circulation around intertropical convergence zones. *J. Atmos. Sci.*, **64**, 2262–2285.
- Peters, L. K., and Coauthors, 1995: The current state and future direction of Eulerian models in simulating the tropospheric chemistry and transport of trace species: A review. *Atmos. Environ.*, **29**, 189–222.
- Pope, C. A., III, D. V. Bates, and M. E. Raizenne, 1995: Health effects of particulate air pollution: Time for reassessment? *Environ. Health Perspect.*, **103**, 472–480.
- Priestley, M. B., 1981: *Univariate Series*. Vol. 1, *Spectral Analysis and Time Series*. Probability and Mathematical Statistics Series, Academic Press, 653 pp.
- Seaman, N. L., 2000: Meteorological modeling for air quality assessments. *Atmos. Environ.*, **34**, 2231–2259.
- Seaton, A., W. MacNee, K. Donaldson, and D. Godden, 1995: Particulate air pollution and acute health effects. *Lancet*, **345**, 176–178.
- Skamarock, W. C., J. B. Klemp, J. Dudhia, D. O. Gill, D. M. Barker, W. Wang, and J. G. Powers, 2005: A description of the Advanced Research WRF version 2. NCAR Tech. Note, NCAR/TN-468+STR, 88 pp.
- Stohl, A., 1998: Computation, accuracy and applications of trajectories—A review and bibliography. *Atmos. Environ.*, **32**, 947–966.
- , G. Wotawa, P. Seibert, and H. Kromp-Kolb, 1995: Interpolation errors in wind fields as a function of spatial and temporal resolution and their impact on different types of kinematic trajectories. *J. Appl. Meteor.*, **34**, 2149–2165.